Near Fields of Thin-Wire Antennas—Computation and Experiment

ARLON TAYLOR ADAMS, SENIOR MEMBER, IEEE, THOMAS E. BALDWIN, JR., SENIOR MEMBER, IEEE, AND DANIEL E. WARREN

Abstract—Techniques for the computation of near fields of thin-wire antennas have been reported in the past. In this paper, the methods for such computation are reviewed, some recent developments are described, and extensive experimental verification is reported. The computed near fields of resonant dipole are compared with experiment. The near fields of broadside and endfire linear arrays are reported. The broadside near-field patterns narrow, whereas the endfire patterns broaden, as distance from the array center increases. Finally, the relevance of near-field computation to near-field radiation hazards and to near-field measurements is discussed.

Key Words: Thin-wire antennas, near fields, computation, experiment, radiation hazards, measurements.

I. INTRODUCTION

THE STUDY of near fields has been of interest to engineers for many years. It has been a difficult study because of the generally complex nature of the near-field structure. Even for thin-wire antennas there are only a few specific cases that have been treated in detail. However, interest in near-field problems has persisted because of the large number of relatively high-power wire antennas and high-grain arrays in use and because of concern with associated problems of electromagnetic compatibility such as coupling, interference, and radiation hazards. In addition, there is interest in improving our basic understanding of near-field phenomena as well.

Moment methods [1], [2] have been used to treat a wide variety of radiation and scattering problems and have also been applied to a number of problems in electromagnetic compatibility [3]. Moment methods for thin-wire near-field computation have been developed and reported in the past [4]. Integral-equation methods for near fields have also been reported [5], [6]. In this paper, the moment methods for thin-wire near-field computation are briefly reviewed, some recent developments are described, and extensive experimental verification is reported. A comparison among several computer programs and with experiment shows generally excellent agreement. The near-field polarization ellipses of a dipole are presented and the computed near fields of a resonant dipole are compared with experiment. The near fields of broadside and endfire linear arrays are shown. The broadside near-field patterns narrow, whereas the endfire patterns broaden, as distance from the array center increases. Near-field radiation hazards are discussed briefly. Radiation hazards are generally greater for endfire than for broadside arrays and are also significantly affected by antenna length and spacing. Finally, near-field measurements are discussed.

Manuscript received July 29, 1976; revised November 1, 1977. This work was supported in part by the Air Force System Command's Rome Air Development Center. A. T. Adams is a participant in the Postdoctoral Program, Rome Air Development Center.

A. T. Adams is with the Department of Electrical and Computer Engineering, Syracuse University, Syracuse, NY 13210. (315) 423-4397.

T. E. Baldwin, Jr., is with the Advanced Program Division, Atlantic Research Corporation, Alexandria, VA 22314.

D. E. Warren is with Compatibility Techniques Section, Rome Air Development Center, Griffiss Air Force Base, Rome, NY 13441.

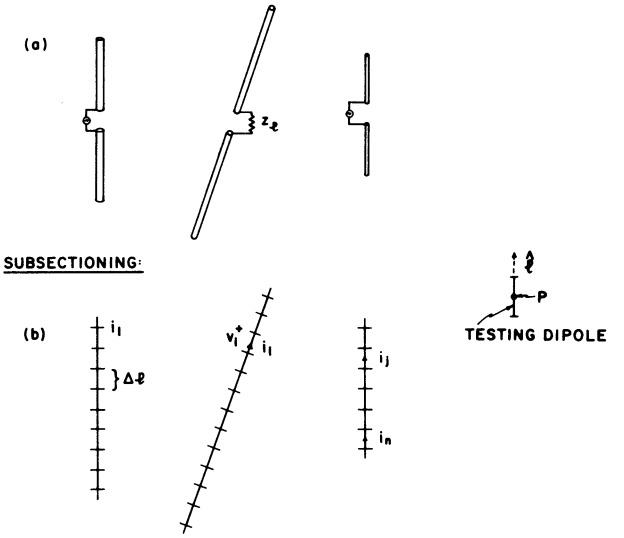

Fig. 1. The method of moments for thin-wire structures.

II. COMPUTATIONAL METHODS FOR NEAR FIELDS

In the method of moments, the computation of near fields proceeds directly from the general formulation. Fig. 1(a) shows a collection of thin-wire ($l \gg a$, $a \ll \lambda$ where l and a are wire length and radius, respectively) antennas, excited and loaded at arbitrary points on the wires. In the method of moments, the antennas are represented by filaments[1] and subsectioned as shown in Fig. 1(b). The currents on the wires are expanded in a sequence of subsectional expansion functions, such as pulses, triangles, sinusoids, etc., [2].

The current is described by a series of complex unknowns $i_1 \cdots i_n$ associated with the expansion functions and representing, for instance, pulse heights or triangle peaks. As a result of this approximation of the current by a finite number of expansion functions, the basic linear integrodifferential equation characterizing the problem is reduced to a matrix

[1] Boundary conditions are applied directly at the wire surface.

0018-9375/78/0200-0259$00.75

equation of the form

$$\begin{bmatrix} v_1 \\ \cdot \\ \cdot \\ \cdot \\ v_n \end{bmatrix} = \begin{bmatrix} z_{11} & \cdots & z_{1n} \\ \cdot & & \cdot \\ \cdot & & \cdot \\ \cdot & & \cdot \\ z_{n1} & \cdots & z_{nn} \end{bmatrix} \begin{bmatrix} i_1 \\ \cdot \\ \cdot \\ \cdot \\ i_n \end{bmatrix} \tag{1}$$

or

$$[v] = [z]\,[i]$$

where v_i represents generalized voltage (a weighted integral of the electric field) and z_{ij} is the generalized impedance.[2]

The matrix methods can be used directly for the computation of near electric- and magnetic-field distributions. Assume that the antenna currents in Fig. 1 have been computed using (1). Now it is required to compute, at a near-field point P (Fig. 1(b)), the near electric-field component in a particular direction $\hat{l}$. It is convenient, for conceptual purposes, to imagine a short thin-wire test dipole located at the near-field point and oriented in the direction $\hat{l}$. An additional expansion function is assumed over the testing wire so that the total number of expansion functions is $(n + 1)$. Now the system of Fig. 1(b) (antenna plus test dipole) is characterized by an expanded z matrix as follows:

$$\begin{bmatrix} v_1 \\ \cdot \\ \cdot \\ \cdot \\ v_{n+1} \end{bmatrix} = \begin{bmatrix} z_{11} & \cdots & z_{1(n+1)} \\ \cdot & & \cdot \\ \cdot & & \cdot \\ \cdot & & \cdot \\ z_{(n+1)1} & \cdots & z_{(n+1)(n+1)} \end{bmatrix} \begin{bmatrix} i_1 \\ \cdot \\ \cdot \\ \cdot \\ i_{n+1} \end{bmatrix}. \tag{2}$$

If the testing wire is open-circuited, $i_{n+1} = 0$ so that

$$v_{n+1} = z_{(n+1)1}i_1 + z_{(n+1)2}i_2 + \cdots + z_{(n+1)n}i_n. \tag{3}$$

An additional row and column of the impedance matrix are thus required; these additional elements represent interactions between the test dipole and the antenna subsections. V_{n+1} is a weighted integral of the electric field over the test dipole of length Δl:

$$V_{n+1} = \int_0^{\Delta l} W_i(l)E_l(l)\,dl \tag{4}$$

where Δl is the length of the test dipole and W_i is a weighting function [2].[3]

For short test dipoles,

$$E_l \cong V_{n+1}\ (\text{open circuit}) \Big/ \int_0^{\Delta l} W_i(l)\,dl \tag{5}$$

$$\Rightarrow V_{n+1}\ (\text{open circuit})/\Delta l\ (\text{for pulse weighting function}). \tag{6}$$

[2] Loading may be taken into account by adding a diagonal load matrix to $[z]$.

[3] For identical weighting and expansion functions, variational expressions for z_{ij} are obtained. In this case, (3) for V_{n+1} offers some possible advantages over direct computation of E_l.

The procedure for computing near fields is to evaluate (5) once for every electric-field-vector component of interest (at each point). Thus E_x, E_y, E_z at a near-field point may be obtained by orienting the test dipole successively in the x, y, z directions and computing (3) and (5) for each component. The current distributions of the actual antennas are computed in the absence of the testing element. This means that the impedance matrix shown in (1) (rather than the expanded matrix of (2)) is used to obtain the antenna current. Near-field results are essentially independent of the particular testing wire used as evidenced by the absence of the self-impedance term $z_{(n+1)(n+1)}$ from (3). A testing dipole of length 0.001λ was used to obtain much of the results reported here.

Thus the near electric field may be obtained by computation of additional impedances. Since a linear relationship analogous to (1) exists between currents and magnetic fields, a similar procedure may be used to compute near magnetic fields once the currents are known. Radiation hazards may also be computed once fields are known (Section VI). Details of the procedures for computing near electric and magnetic fields are given in the literature [4], [7]. There are a number of possible variations on the techniques described above.

Near-field techniques, such as those described above, permit one to compute near fields accurately as close as one subsection from the wire surface (and even closer in some cases).

Near-field phenomena are often of a complex nature. Furthermore, the present knowledge and understanding of near-field effects are somewhat incomplete. Therefore, it is desirable to be able to obtain checks on near-field computations. Several methods have been devised and have proven useful in checking computations. In many cases, the approximate form and magnitude of current is known. The fields computed from the currents may then be checked by a generalization of Ampere's and Gauss' Laws [4] in regions close to the individual wires and by Hertzian-dipole approximations in more distant regions. Typical results of such checks show good agreement with direct computation of (5).

Computation of near-field data may be time-consuming if a large number of near-field points is required. Computation can be speeded considerably by using a Hertzian-dipole model where appropriate. The current-carrying subsection is replaced with one or more Hertzian dipoles of appropriate current moments. A study has been made of the accuracy of the Hertzian-dipole model, as compared with the complete method of (5). The Hertzian-dipole formulation is used to compute the contribution of current-carrying subsections whose distances from the near-field point are greater than some specified distance (which is normally chosen to be 0.2λ). A comparison of this combined method with the original method shows less than 1-percent difference or error. In some typical computations of the near fields of arrays, the computation time is thereby reduced by a factor greater than 15. The computer program of [8] incorporates this method.

III. THE NEAR-FIELD POLARIZATION ELLIPSE

The general behavior of the electric- and magnetic-field vectors at a near-field point can be described as follows: for

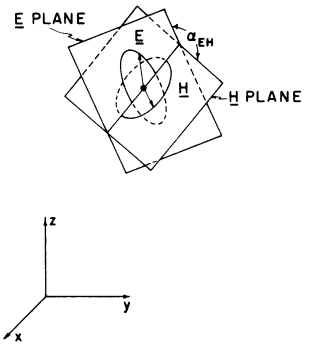

Fig. 2. Near-field $\bar{E}$ and $\bar{H}$ polarization ellipses.

time-harmonic problems in the near-field, there are, in general, three orthogonal components of the electric field with arbitrary relative amplitudes and phases. The tip of the resultant electric vector traces out an ellipse lying in an arbitrary plane (Fig. 2). The magnetic vector traces out a different ellipse lying in a different plane. Thus there is a particular local coordinate system in which there are only two components of the electric field and another in which there are only two components of the magnetic field.

This behavior may be understood by noting that, if the electric field, for instance, is resolved into quadrature components, then each of the two quadrature components represents a linearly polarized vector. The resultant is thus an ellipse lying in the plane common to the two lines traced out by the quadrature components. Once the three complex components of the electric or magnetic field have been computed, the complete characteristics of the ellipse, including rms and peak values, and major and minor axes of the ellipse, may be determined by methods outlined in [7].

Fig. 3(a) shows the near-field polarization ellipses for a z-directed, centered, half-wave dipole of radius $a = 0.005\lambda$, centered at the origin, as a function of cylindrical coordinates ρ and z, in a constant-ϕ plane. For a dipole, the electric-field ellipse lies in a constant-ϕ plane and the magnetic field is linearly polarized.[4] The electric field becomes linearly polarized for $z = 0$, for large $r = \sqrt{\rho^2 + z^2}$, and for points near the dipole (except at the gap and ends). The behavior near gap and ends is shown in [4]. Fig. 3(b) shows a plot of the axial ratio (major axis/minor axis) as a function of ρ and z, for the same antenna. Note that, for most values of z/λ, there is a point where the axial ratio is nearly equal to unity. The components are nearly 90° out of phase at this point, leading to circular polarization. Note that there is a path of nearly circular polarization in the near field, starting along a line $z = \rho(\theta = 45°)$ and curving off to the left (small values of θ). This near-field behavior corresponds roughly to that of the Hertzian dipole (the condition for circular polarization for the Hertzian dipole is $\sin\theta = 2/kr$, $kr \gg 1$).

The theory of the near-field polarization ellipse may be applied to such near-field problems as radiation hazards and coupling effects. Radiation hazards may be related to the

[4] For arrangements of two or more dipoles, or for a single bent wire, the orientation of the polarization ellipse is nontrivial and must be determined by computation.

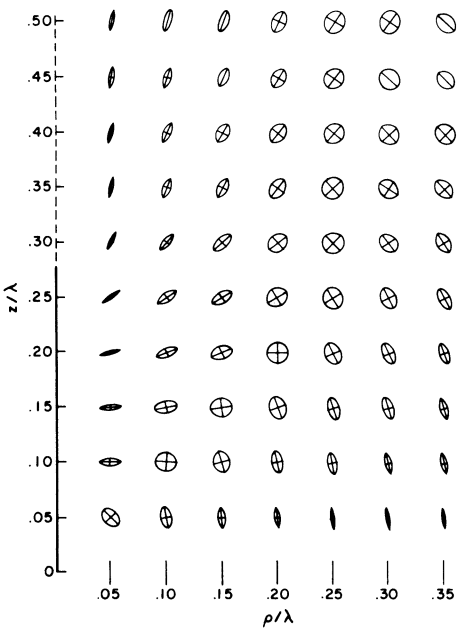

(a)

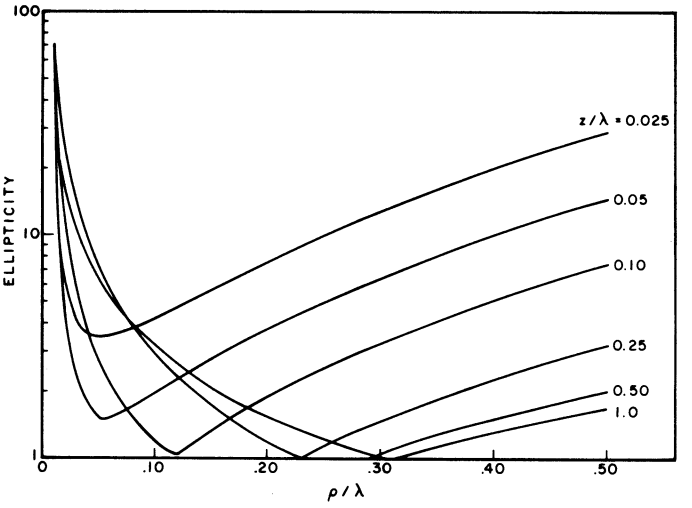

(b)

Fig. 3. Near-field polarization of a half-wave dipole ($l = 0.5\lambda$, $a = 0.005\lambda$). (a) Near-field ellipses. (b) Axial ratio.

mean-square and peak values of field quantities as described in [7]. Knowledge of the major axis of the ellipse may be used to predict antenna orientation for maximum near-field coupling. For short dipoles in an arbitrary time-harmonic field, there is always one orientation for zero, or nearly zero, coupling; namely, with the dipole perpendicular to the plane of the polarization ellipse.

IV. NEAR FIELDS OF A DIPOLE

The near fields E_ρ, E_z of a centerfed, z-directed, resonant, half-wave dipole, at a distance of about three wire diameters from the axis, are shown in Fig. 4(a), (b), respectively. The voltage excitation is 1 V. Three different computer programs [8]-[10] labeled methods 1, 2, 3, respectively, are used and their results compared with experimental data. All three computer programs are based on the method of moments. Methods

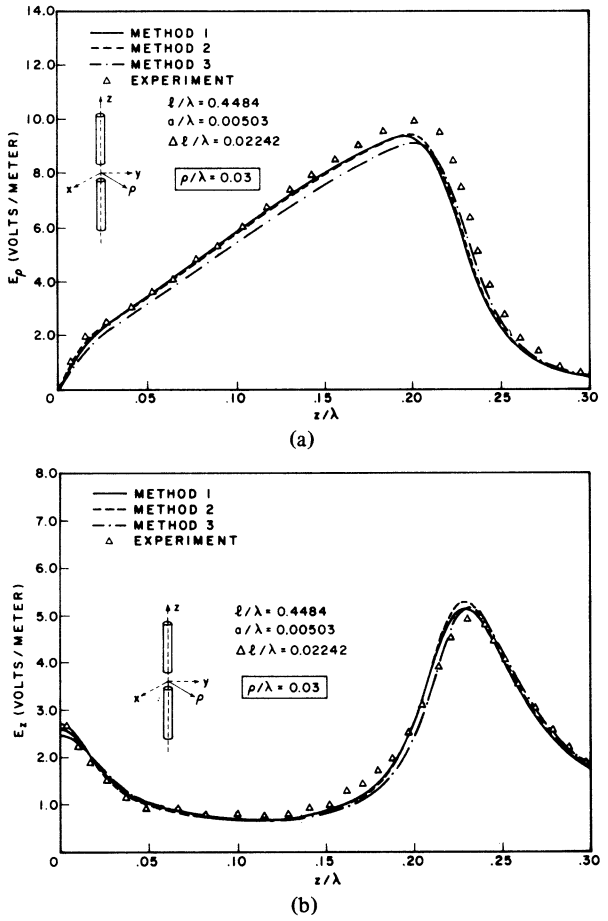

Fig. 4. Near fields of a resonant dipole ($l = 0.4484\lambda$, $a = 0.00503\lambda$). (a) E_ρ. (b) E_z.

1, 2, 3 utilize pulse, triangular, and modified sinusoidal expansion functions, respectively. The experimental data were measured with a short E-field probe connected to instrumentation (digital voltmeter) by a twisted pair of high-resistance wires. The experimental setup is described in detail in [11]. Note the excellent agreement among computer methods and with experiment. Extensive additional measured data for larger ρ/λ and for nonresonant dipoles ($l/\lambda = 0.25, 0.49$) also shows good agreement with computation.

Additional computed data [4] on dipole near fields show good agreement between computer methods for points closer to the dipole than those shown in Fig. 4(a), (b). In this region, special calibration procedures would be required for measurement (see Section VII). Good agreement is also obtained with the Ampere's and Gauss' Law results [4]. In regions very close to the dipole, E_ρ has approximately a $(1/\rho)$ dependence and E_z has approximately a $(\ln \rho/a)$ dependence, except near the gap and ends of the antenna. Both E_z, E_ρ peak sharply near the gap and end regions.

The current is approximated by a finite set of expansion functions which, of course, do not represent exactly the true current. Computations of fields at points extremely close to the dipole surface show spurious periodic perturbations corresponding to the subsectioning. Such spurious results showed up in our computations at distances of about one-quarter wire diameter from the dipole surface.

The excellent agreement shown in these and other examples leads us to conclude that the near-field methods used are accurate as close as the length of one subsection from the wire surface.

V. NEAR FIELDS OF LINEAR ARRAYS

The near fields of linear arrays of dipoles have been studied using Method 1. Fig. 5(a) (inset) shows a linear eight-element array of dipoles with a uniform length l and spacing d. The dipoles are centered on the x axis and centerfed. The computations shown here were made for $l = d = \lambda/2$ in the principal H-plane, with either a) broadside or b) endfire excitation. Ten subsections per dipole were used.

Fig. 5(a) shows the normalized near-field patterns for broadside (uniform) excitation. Note that the beam patterns smoothly and gradually approach the far-field pattern with the peaks and nulls forming gradually and the main beam narrowing as distance ρ to the field point increases. The positions of the peaks and nulls in the near field correspond approximately to those of the far field. The outer sidelobes form more rapidly as ρ increases. All mutuals are taken into account and thus the far-field pattern differs from the classical pattern of an array of Hertzian dipoles.

Fig. 5(b) shows the normalized near-field beam patterns for endfire excitation (adjacent dipoles are excited with a phase difference of π radians). In contrast to the broadside case (Fig. 5(a)) the mainbeam broadens as ρ increases. This can be explained solely in terms of the geometry and excitation. For instance, for ρ close to 1.75λ, and ϕ close to zero, the distance from the nearest dipole increases very rapidly as ϕ increases. As a result, the field strength decreases very rapidly with ϕ, leading to a narrower beam than would be obtained with larger ρ. Also, the contributions from the nearest two neighbors change very rapidly from constructive to destructive interference as ϕ increases from zero (more rapidly than would be the case for larger ρ). The contrasting effect in the broadside case can be explained by a similar heuristic analysis. The patterns of Fig. 5(b) smoothly and gradually approach the far-field pattern, except that crossover is required because of the broadening of the beam with increasing ρ. The peaks and nulls form very rapidly with increasing ρ (compare with Fig. 5(b)). Since mutuals are taken into account, the far-field pattern differs slightly from that of the classical case.

Fig. 6 shows the electric-field strength at points closer to the array. A rectangular coordinate plot is used in contrast to the polar coordinate plot used in Fig. 5. Fig. 6(a) shows the electric-field strength for uniform (broadside) excitation. The field strength is nearly uniform across the face of the array and tapers off rapidly near the end ($x = 1.75\lambda$) of the array. Sharp peaks at x coordinates corresponding to the locations of the dipoles occur only for $y = 0.05\lambda$. This situation is in contrast to the electric field of short isolated dipoles (not shown) which has sharp peaks at greater values of y. The "smoothing out" of the pattern is related to the geometry and can be accentuated or diminished by varying l and d [7]. As l decreases from 0.5λ to 0.25λ, the region of sharp peaks moves out from $y = 0.05\lambda$ to 0.15λ. A decrease in spacing d has the opposite effect [7].

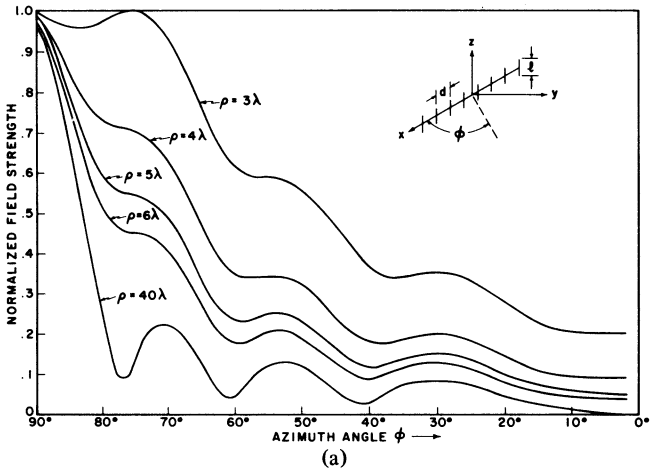

(a)

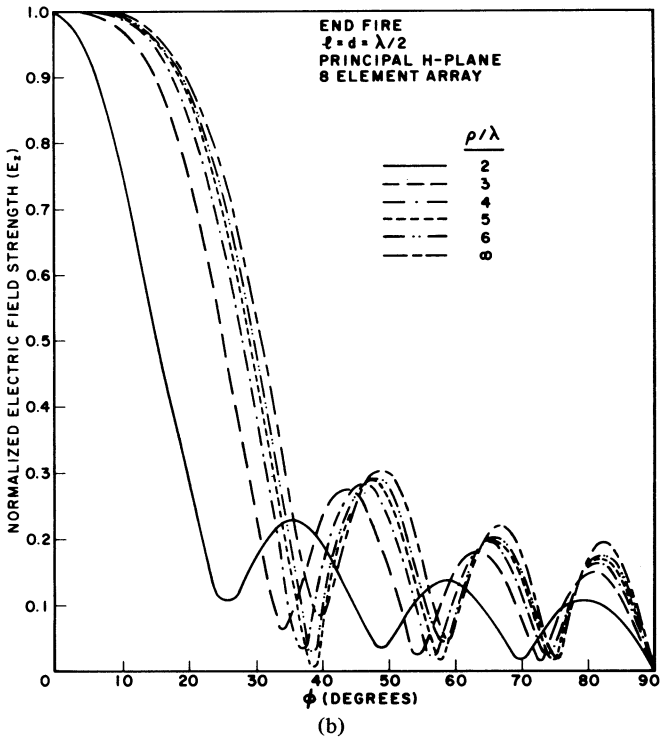

(b)

Fig. 5. Principal H-plane near fields of an eight-element linear array ($l = d = 0.5\lambda$, $a = 0.005\lambda$)—polar coordinate plot. (a) Uniform excitation. (b) Endfire excitation.

Fig. 6(b) shows the electric-field strength for endfire excitation. Peaks occur near the z-coordinate locations of the individual dipoles. Because of the phase shift of π radians between adjacent dipoles, deep nulls occur at x-coordinate positions halfway between individual dipoles. Thus the "peaking" effect is more noticeable in the endfire case. Null depth increases with increasing distance y from the array, and also decreases with increasing x. Fig. 6(c) shows the falloff pattern maxima for Figs. 5(b), 6(b) as a function of ρ. Note that the falloff closely approximates a $(1/\rho)$ dependence, except in a region close to the array ($\rho < 4\lambda$) where falloff is less rapid due to the physical extent of the array. Additional near-field data for larger and smaller arrays and for Chebyshev excitation are given in [7]. An experimental check of near fields for two-element arrays shows good agreement with computation [11]. Radiation hazard data for arrays are given in Section VI.

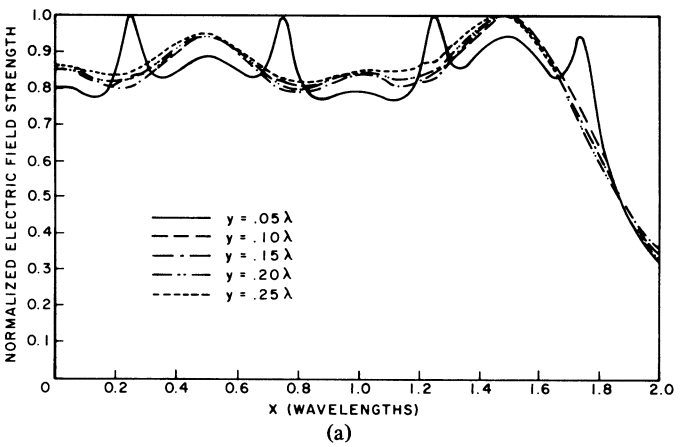

(a)

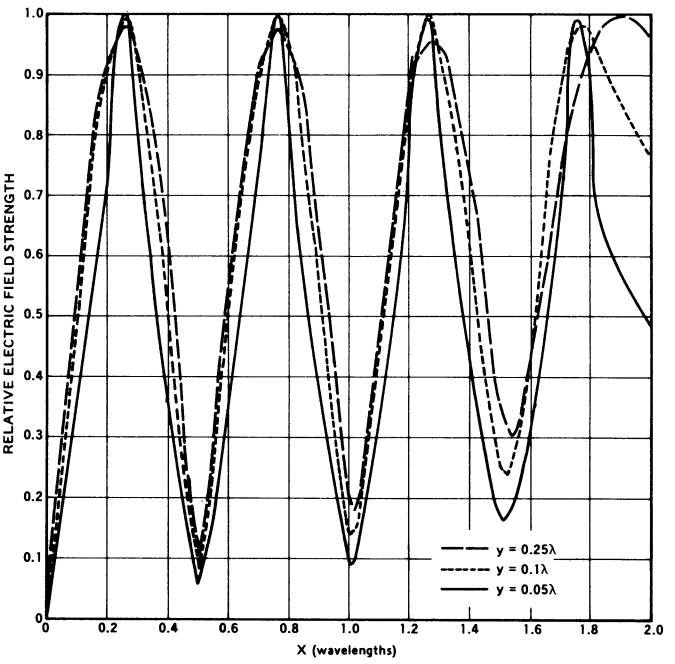

(b)

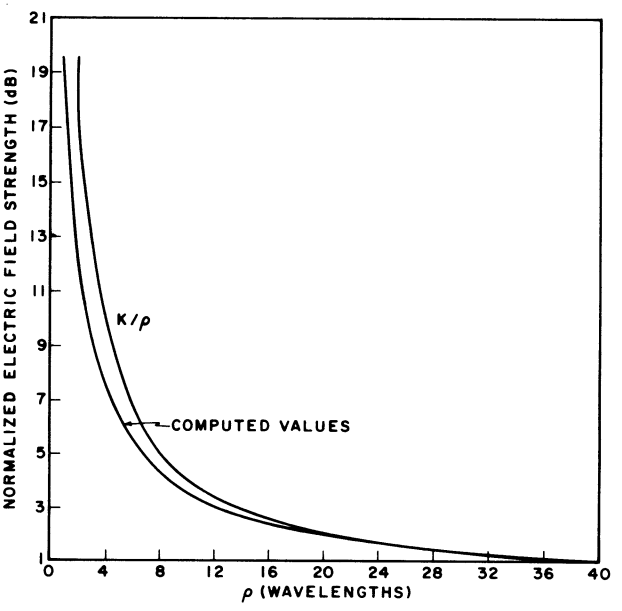

(c)

Fig. 6. Principal H-plane near fields of an eight-element linear array of dipoles ($l = d = 0.5\lambda$, $a = 0.005\lambda$)—rectangular coordinate plot. (a) Uniform excitation. (b) Endfire excitation. (c) Falloff of maxima.

VI. RADIATION HAZARDS IN THE NEAR FIELD

Once the complex electric and magnetic fields have been computed, the evaluation of radiation hazards may be considered. Researchers agree, with certain reservations, that radiation damage is primarily a heating effect.

Consider the instantaneous electric field at a near-field point for the time-harmonic case:

$$\epsilon(x, y, z, t) = \hat{x}E_x \cos(\omega t + \alpha_x) + \hat{y}E_y \cos(\omega t + \alpha_Y) + \hat{z}E_z \cos(\omega t + \alpha_z). \tag{7}$$

The near-field phasor-vector $\boldsymbol{E}(x, y, z)$ may then be expressed as:

$$\boldsymbol{E}(x, y, z) = \hat{x}\frac{E_x}{\sqrt{2}}e^{j\alpha x} + \hat{y}\frac{E_y}{\sqrt{2}}e^{j\alpha y} + \hat{z}\frac{E_z}{\sqrt{2}}e^{j\alpha z} \tag{8}$$

where

$$\epsilon(x, y, z, t) \triangleq \mathrm{Re}\sqrt{2}E(x, y, z)e^{j\omega t}.$$

The time-average of the square of the length of the instantaneous electric vector $\epsilon(x, y, z, t)$ is

$$\tfrac{1}{2}(E_x^2 + E_y^2 + E_z^2) \qquad \text{(see [7])}.$$

Now define

$$|\boldsymbol{E}|^2 = |\boldsymbol{E}(x, y, z)|^2 \triangleq \tfrac{1}{2}(E_x^2 + E_y^2 + E_z^2). \tag{9}$$

Then the heat dissipation within a volume v may be expressed as [12]

$$W = \iiint_v [(\sigma + \omega\epsilon'')|\boldsymbol{E}|^2 + \omega\mu''|\boldsymbol{H}|^2]\, dv. \tag{10}$$

If dielectric and conductive losses predominate and if, in addition, the electric field and material constants are uniform over v, then

$$W = (\sigma + \omega\epsilon'')(\text{volume})|\boldsymbol{E}|^2. \tag{11}$$

A proper criterion in those cases where (11) applies would be an electric-field criterion. Thus if 10 mW/cm^2 is a valid power criterion in the far field with a single plane-wave incident, then

$$|E| = 194 \text{ V/m (rms)} \tag{12}$$

would be an equally valid electric-field criterion in the near field for those cases where (11) applies. Equations (11) and (12) may be used for those cases where the heating effect is the important radiation hazard. For effects dependent upon peak values of the electric field, the peak values of electric field may be computed directly.

The relevance of near-field computation is as follows. For thin-wire structures, the electric near field may be computed and compared with an appropriate criterion such as (12). For more precise analysis, based on (10), one may determine by moment methods the currents, charges, fields, and dissipation in the presence of a dissipative object in the near field, if the object can be modeled as one or more wires loaded with complex impedances.

There has been considerable discussion concerning the appropriate level for (12) and whether it should be a function of frequency. A level independent of frequency may be too conservative at some frequencies and too liberal at others. For instance: at low frequencies, humans often work in electric fields of very high intensity without noticeable damage. The reason, of course, is that humans are electrically small scatterers at these frequencies. For electrically small scatterers, induced currents are proportional to ω (radian frequency) and dissipation is proportional to ω^2 or $\omega^{5/2}$ depending on skin depth [7]. Induced charge densities are essentially independent of frequency. Logically, radiation-hazard criteria should involve a corresponding correction factor for electrical size.[5]

One might expect that sharp peaks in the near field (such as those shown in Fig. 6(a), (b)) would indicate a possible radiation hazard. This indeed turns out to be the case, In some cases, the radiation hazard is increased considerably if the length l is shortened. For instance, in the broadside case for the eight-element array of Fig. 5(a), decreasing the length l from 0.5λ to 0.25λ increases the radiation hazard by a factor of 35, at a location 0.05λ distant from one of the central dipoles, with 1-W net input power in each case. Similar effects are noted in the endfire case. Radiation hazards are generally greater in the endfire case because of the sharper peaks and nulls (Fig. 6(b)).

Computer program [8] has an option which computes and prints out radiation- hazard levels over a rectangular grid. The radiation hazards are proportional to the sum of the squares of the magnitudes of the electric-field vectors [7]. Contour plots can readily be derived from these data. Fig. 7 shows a contour plot in the principal H-plane for the eight-element broadside array ($d = l = 0.5\lambda$). All elements are center-driven with 1-V excitation. Input power to the array is 0.133 W. The radiation hazard criterion is 10 mW/cm^2 or 194 V/m and hazard contours are plotted in dB relative to this level. Note that the partially formed peaks and nulls of the near-field pattern (Fig. 5(a)) show up clearly in the plot of Fig. 7, forming progressively (as ρ increases) at angles corresponding to peaks and nulls of the far-field pattern. The principal H-plane ($z = 0$) is a special case, albeit one of principal interest for large vertical arrays (in the principal H-plane there is only one component E_z of the electric field). It is interesting to note that the radiation-hazard contours vary slowly as a function of z. Plots for $z = 0, 0.125\lambda$ show very little difference in hazard levels (there is a maximum difference of 5 dB for all the data points of Fig. 7). This would

[5] It should also be noted that charge buildup and resulting polarization stress is independent of electrical size; there may be some low frequency at which polarization stress dominates.

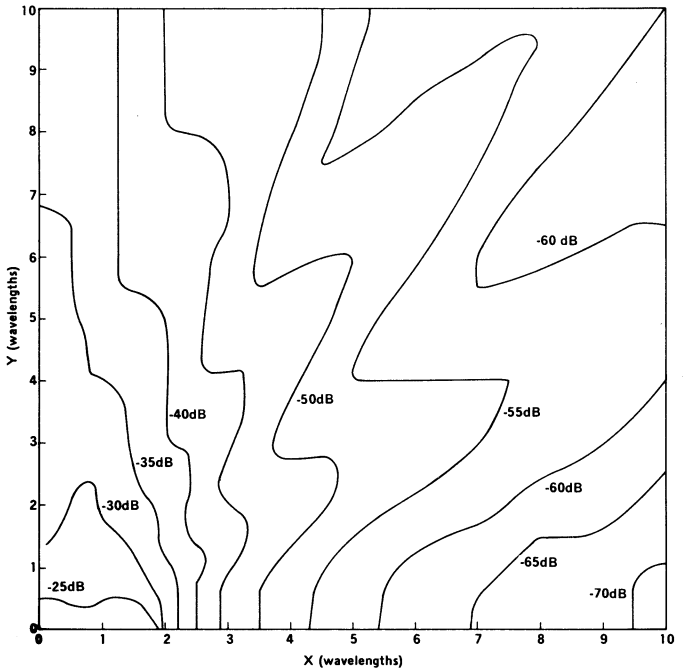

Fig. 7. Radiation-hazard contours in the principal H-plane of a uniformly excited eight-element linear array of dipoles ($v = 1$ V, $l = d = 0.5\lambda$, $z = 0$).

probably not be the case if the data were computed very near the individual dipoles.

VII. NEAR-FIELD MEASUREMENTS

Measurements in the near field are affected by interactions among the measuring instrument and other nearby objects. Fig. 8 shows the degree of this interaction for small test dipoles sampling the near field of a half-wave dipole. The radiating-dipole dimensions are l_1, a_1 and the test-dipole dimensions are l_2, a_2. For each case, the open-circuit voltage at the test antenna terminals (computed in the presence of the test antenna) is compared with the computed near field at the test antenna location (in the absence of the test antenna). All quantities are computed by the method of moments. Near fields are computed by the methods described in Section II. The open-circuit voltage is obtained by a method-of-moments solution in the presence of the test antenna, in which case, voltages and currents at the two terminals are related as follows:

$$V_1 = Z_{11}I_1 + Z_{12}I_2$$
$$V_2 = Z_{12}I_1 + Z_{22}I_2 \tag{13}$$

where Z_{11}, Z_{12}, Z_{22} are the conventional open-circuit impedance parameters of network theory.

Let $V_1 = 1, V_2 = V_{0c}, I_2 = 0$. Then,

$$V_2 = V_{0c} = Z_{12}/Z_{11}. \tag{14}$$

The open-circuit voltage is thus obtained from the open-circuit impedance parameters, which in turn can be obtained from the generalized impedance matrix $[z]$ of the method of moments by selecting the four elements of $[y] = [z]^{-1}$ corresponding to the terminals and inverting the resulting 2×2 matrix [3].

Fig. 8(a) shows the resulting ratio V_{0c}/l_2E_z as the vertical test dipole approaches the radiating half-wave dipole, as a function of vertical position z/λ for a test dipole of length $l_2 = 0.1\lambda$. Note that the curves diverge significantly for $\rho < 0.1\lambda$, indicating a strong interaction and one which varies according to position z/λ. The interaction is strongest near the gap ($z = 0$) and ends ($z = 0.25$) of the dipole, because the near field E_z (in the absence of the test dipole) is strongest there. Fig. 8(b) shows the corresponding data for a horizontal test dipole. Note that interactions again become significant in the region $\rho < 0.1\lambda$.

For large values of ρ, the ratios V_{0c}/l_2E_z and V_{0c}/l_2E_x of Fig. 8 converge to about 0.47, which is close to the theoretical value of 0.5 expected from classical theory. This limiting value, of course, depends slightly on l_2, a_2; it appears to approach 0.5 for very thin wires.

For a smaller test dipole of length $l_2 = 0.01\lambda = 100\,a_2$, the interaction becomes significant for $\rho < 0.05\lambda$.

Plots such as those in Fig. 8, generated by the method of moments, can be used to indicate the significance of interactions in a given near-field configuration and, correspondingly, the accuracy of near-field measurements based on far-field calibration.[6]

VIII. SUMMARY

Numerical methods for the computation of near fields of thin-wire antennas and scatterers have been described. Comparative data on typical problems indicate the method to be accurate as close as the length of one subsection from the wire surface. Methods of checking and simplifying near-field computations were noted. The near-field polarization ellipse and near fields of a half-wave dipole were presented. The near fields of broadside and endfire arrays were described in detail. The broadside near-field patterns narrow, whereas the endfire patterns broaden as distance r increases. The peaks and nulls of the endfire array form more rapidly than those of the broadside array as r increases. The near fields of an array and the resultant radiation hazards are significantly affected by geometry and excitation. Radiation hazards are more severe for the endfire than for the broadside arrays. Radiation hazard criteria and near-field measurements were briefly discussed.

ACKNOWLEDGMENT

The authors wish to acknowledge useful conversations with Dr. B. J. Strait, Dr. R. F. Harrington, and Dr. J. R. Mautz. The measurements were performed by R. Robertson of Atlantic Research Corporation. Many thanks to E. Caldeira for his assistance in some of the computations.

[6] Near-field calibration data could also be derived, but the corrections vary significantly according to position, as indicated by the data of Fig. 8.

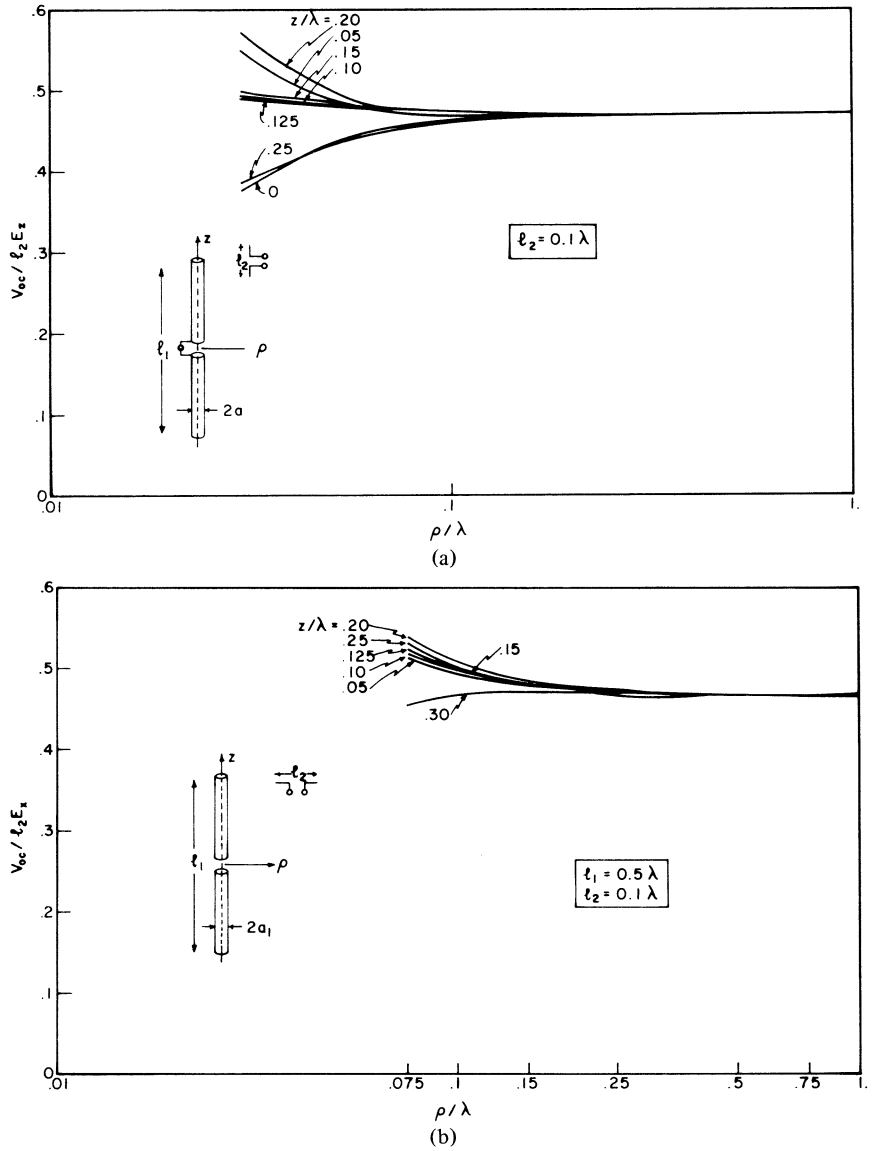

Fig. 8. Near-field open-circuit voltage calculations. (a) V_{oc}/l_2E_z. (b) V_{oc}/l_2E_x.

REFERENCES

[1] R. F. Harrington, "Matrix methods for field problems," *Proc. IEEE*, vol. 55, no. 2, Feb. 1967, pp. 136–149.

[2] R. F. Harrington, *Field Computation by Moment Methods.* New York: Macmillan Co., 1968.

[3] B. J. Strait and A. T. Adams, "Analysis and design of wire antennas with applications to EMC," *IEEE Trans. Electromag. Compat.*, vol. EMC-12, no. 2, May 1970, pp. 45–54.

[4] A. T. Adams, B. J. Strait, D. E. Warren, D. Kuo, and T. E. Baldwin, Jr., "Near fields of wire antennas by matrix methods," *IEEE Trans. Antennas Propagat.*, vol. AP-21, no. 5, Sept. 1973, pp. 602–610.

[5] R. W. P. King and T. T. Wu, "Currents, charges and near-fields of cylindrical receiving and scattering antennas," *IEEE Trans. Antennas Propagat.*, vol. AP-13, 1965, p. 973.

[6] C. W. Harrison, Jr., C. D. Taylor, E. A. Aronson, and M. L. Houston, "An accurate representation of the complete electromagnetic field in the vicinity of a base-driven cylindrical monopole," *IEEE Trans. Electromag. Compat.*, vol. EMC-12, no. 4, Nov. 1970, pp. 164–173.

[7] A. T. Adams, T. E. Baldwin, Jr., D. E. Warren, and E. Mendelovicz, "Near fields of thin-wire antennas," RADC Method of Moments Applications, Vol. II, RADC-TR-73-217 (II), Aug. 1973, AD 767907.

[8] D. E. Warren, T. E. Baldwin, and A. T. Adams, "Near electric and magnetic fields of wire antennas," *IEEE Trans. Antennas Propagat.*, vol. AP-22, no. 2, Mar. 1974, p. 364. Program and description on deposit: ASIS-NAPS Document No. NAPS-02221.

[9] D. C. Kuo, H. H. Chao, J. R. Mautz, B. J. Strait, and R. F. Harrington, "Analysis of radiation and scattering by arbitrary configurations of thin wires," *IEEE Trans. Antennas Propagat.*, vol. AP-20, no. 6, Nov. 1972, pp. 814–815. Program and description on deposit: ASIS-NAPS Document No. NAPS-01798.

[10] Antenna Modeling Program: Engineering Manual (Report IS-R-72/10, July 1972), User Manual (Report IS-R-72/15, July 1973), Systems Manual (Report IS-R-72/10, April 1973) Information Systems Division of MB Associates, Menlo Park, CA.

[11] T. E. Baldwin, "Thin-wire antenna analysis computer codes compared with measured data," RADC Method of Moments Applications, Vol. V, RADC-TR-73-217 (V), July 1974, AD 783-897.

[12] R. F. Harrington, *Time-Harmonic Electromagnetic Fields.* New York: McGraw-Hill, 1961, pp. 24–25.